

Oncogenic KRAS-expressing organoids with biliary epithelial stem cell properties give rise to biliary tract cancer in mice

Akiyoshi Kasuga^{1,2}  | Takashi Semba^{1,3} | Ryo Sato^{1,4} | Hiroyuki Nobusue¹ | Eiji Sugihara^{1,5}  | Hiromasa Takaishi² | Takanori Kanai² | Hideyuki Saya¹ | Yoshimi Arima¹ 

¹Division of Gene Regulation, Institute for Advanced Medical Research, Keio University School of Medicine, Tokyo, Japan

²Division of Gastroenterology and Hepatology, Department of Internal Medicine, Keio University School of Medicine, Tokyo, Japan

³Department of Thoracic Surgery, Kumamoto University, Kumamoto, Japan

⁴Department of Respiratory Medicine, Kumamoto University, Kumamoto, Japan

⁵Research and Development Center for Precision Medicine, University of Tsukuba, Ibaraki, Japan

Correspondence

Yoshimi Arima, Division of Gene Regulation, Institute for Advanced Medical Research, Keio University School of Medicine, 35 Shinano-machi, Shinjuku-ku, Tokyo 160-8582, Japan.
Email: arima@z7.keio.jp

Funding information

Grants-in-Aid for Scientific Research from the Ministry of Education, Culture, Sports, Science, and Technology of Japan, Grant/Award Number: KAKENHI 20K08968 and KAKENHI 22130007; Translational Research Network Program, Research on Applying Health Technology, and Research on Rare and Intractable Diseases grants from the Japan Agency for Medical Research and Development; Keio Gijyuu Academic Development Funds

Abstract

Biliary tract cancer (BTC) arises from biliary epithelial cells (BECs) and includes intrahepatic cholangiocarcinoma (IHCC), gallbladder cancer (GC), and extrahepatic cholangiocarcinoma (EHCC). Although frequent *KRAS* mutations and epigenetic changes at the *INK4A/ARF* locus have been identified, the molecular pathogenesis of BTC is unclear and the development of corresponding anticancer agents remains inadequate. We isolated epithelial cell adhesion molecule (EPCAM)-positive BECs from the mouse intrahepatic bile duct, gallbladder, and extrahepatic bile duct, and established organoids derived from these cells. Introduction of activated *KRAS* and homozygous deletion of *Ink4a/Arf* in the cells of each organoid type conferred the ability to form lethal metastatic adenocarcinoma with differentiated components and a pronounced desmoplastic reaction on cell transplantation into syngeneic mice, indicating that the manipulated cells correspond to BTC-initiating cells. The syngeneic mouse models recapitulate the pathological features of human IHCC, GC, and EHCC, and they should therefore prove useful for the investigation of BTC carcinogenesis and the development of new therapeutic strategies. Tumor cells isolated from primary tumors formed organoids in three-dimensional culture, and serial syngeneic transplantation of these cells revealed that their cancer stem cell properties were supported by organoid culture, but not by adherent culture. Adherent culture thus attenuated tumorigenic activity as well as the expression of both epithelial and stem cell markers, whereas the expression of epithelial-mesenchymal transition (EMT)-related transcription factor genes and mesenchymal cell markers was induced. Our data show that organoid culture is important for maintenance of epithelial cell characteristics, stemness, and tumorigenic activity of BTC-initiating cells.

KEYWORDS

biliary tract cancer, cancer stem cell, cholangiocarcinoma, epithelial-mesenchymal transition, organoid culture

This is an open access article under the terms of the Creative Commons Attribution-NonCommercial License, which permits use, distribution and reproduction in any medium, provided the original work is properly cited and is not used for commercial purposes.

© 2020 The Authors. *Cancer Science* published by John Wiley & Sons Australia, Ltd on behalf of Japanese Cancer Association.

1 | INTRODUCTION

Biliary tract cancer (BTC) arises from biliary epithelial cells (BECs) lining the bile duct and can occur in distinct anatomic locations. It thus includes intrahepatic cholangiocarcinoma (IHCC), extrahepatic cholangiocarcinoma (EHCC), and gallbladder cancer (GC). Although the incidence of BTC remains highest in Asia and parts of South America, the rate of IHCC has been rising globally—including in North America, Europe, Australia, and Japan—over the past 2 decades.^{1,2} The prognosis of individuals with advanced BTC is poor, with a median survival time of ~12 months and a 5-year survival rate of ~2%.³ Indeed, the disease is usually diagnosed only after it has reached the advanced stage. There are few promising anticancer agents for BTC, which is usually treated with gemcitabine, cisplatin, or S-1. New therapeutic options and markers that allow for early detection or inform personalized treatment are therefore urgently needed for BTC.

Molecular studies have identified frequent alterations in *KRAS* and at the *INK4A/ARF* locus in human BTC. *KRAS* and *TP53* are the 2 genes most frequently mutated in IHCC, and *KRAS* mutations have been detected in ~30% of BTC tumors.⁴ The tumor suppressor gene *INK4A*, which encodes the cyclin-dependent kinase inhibitor p16, was found to be inactivated in up to 80% of cholangiocarcinomas, with the most frequent mechanism of inactivation being the loss of transcription as a result of DNA methylation at a CpG island in the promoter region.^{5,6}

Genetically engineered mouse models can provide important insight into the molecular pathogenesis of human diseases and allow preclinical assessment of potential therapeutic strategies. The generation of transgenic mouse models for BTC has been limited, however. Although some mouse models for cholangiocarcinoma with liver-specific oncogene activation have been established, most of these mice develop hepatocellular carcinoma as well as IHCC.^{7,8} Mouse models engineered with the use of the cytokeratin 19 (CK19) gene promoter develop not only cholangiocarcinoma but also neoplastic lesions in a variety of tissues including pancreatic ducts, gastric and colonic mucosa, and lung.^{9,10} Recently, several organoid-based mouse models of human IHCC, EHCC, and GC have been established and have shed light on the pathogenesis of human BTC.^{9,11-14} Organoid culture is a type of 3D culture that supports the formation of budding, cystlike structures from stem cells.¹⁵ Organoid models of the normal small intestine, colon, liver, and pancreas of mice have been established.¹⁵⁻²⁰ Epithelial cell adhesion molecule (EpCAM) is a cell surface protein that contributes to cell-cell adhesion and is expressed in normal epithelial tissues and epithelium-derived tumors. EpCAM-positive cells isolated from the normal liver have been found to contain hepatic stem cells.²¹⁻²⁴

Cancer stem cells (CSCs) are a subpopulation of tumor cells that possess high tumorigenic activity and represent the top of a hierarchical organization similar to that of normal tissues. Similar to normal tissue stem cells, CSCs also possess self-renewal capacity and multipotency.^{25,26} We previously established induced CSCs (iCSCs) from mouse somatic stem or progenitor cells of various

tissues by forced expression of a set of defined factors.²⁷ With the use of retroviral transduction of driver genes such as *MYC* or *RAS*, we have thus generated several types of iCSCs—including those for osteosarcoma, choriocarcinoma, glioblastoma, ovarian cancer, and leukemia-lymphoma—that are capable of forming tumors on transplantation into recipient syngeneic mice. The phenotypes of these iCSC-derived tumors—including excessive growth, intratumoral heterogeneity, and invasive-metastatic ability—recapitulate those of the corresponding human cancers.

In the present study, we have combined 3D organoid culture with transplantation of oncogenic *KRAS*-expressing BECs into syngeneic mice. We thereby generated mouse models of BTC (IHCC, GC, and EHCC) that are based on transplantation of syngeneic tumor-initiating cells (TICs) derived from organoids formed by EpCAM-positive BECs. These TICs manifested epithelial stem cell characteristics and a high tumorigenic activity. The developed tumors were aggressive and were associated with a desmoplastic reaction, thus recapitulating the pathological features of human tumors. The stromal desmoplasia of tumor tissue included ECM, fibroblasts, endothelial cells, and infiltrated immune cells, indicating that the tumor microenvironment interacted and cooperated with BTC cells in our mouse models. Preclinical studies with these mouse models may lead to the development of more effective therapeutic agents for BTC.

2 | MATERIALS AND METHODS

2.1 | Mice

All mouse experiments were approved by the ethics committee of Keio University School of Medicine (approval number 17034), and the animals were treated in compliance with the regulations for animal experiments of Keio University School of Medicine. Six- to 8-week-old WT C57BL/6J mice served as immunocompetent recipients of cell transplants. WT C57BL/6J mice and *Ink4a/Arf*-null C57BL/6J mice (B6.129-Cdkn2atm1Rdp; NCI, Frederick, MD, USA) were used for the establishment of BEC organoids.

2.2 | Isolation of BECs

For isolation of BECs from the intrahepatic bile duct (IHBD), gallbladder (GB), or extrahepatic bile duct (EHBD), the liver, GB or EHBD of 6-week-old female mice was minced with a razor blade and incubated for 45 minutes at 37°C in a digestion solution consisting of collagenase D (2 mg/mL; Sigma-Aldrich), dispase II (0.125 mg/mL, Sigma-Aldrich), and DNase I (0.1 mg/mL, Sigma-Aldrich) in DMEM-F12 (Wako). The digested tissue was filtered through a 40- μ m nylon cell strainer (BD Biosciences), the filtrate was centrifuged at 400 \times g for 5 minutes, and the resulting cell pellet was suspended in TrypLE solution (DNase I [0.1 mg/mL, Sigma-Aldrich] in TrypLE Express [Life Technologies]) and incubated for

5 minutes at 37°C. The suspension was then filtered through a 40- μ m nylon cell strainer, the filtrate was centrifuged at 400 \times g for 5 minutes, and red blood cells in the pellet were lysed by the addition of 150 mmol/L NH_4Cl . The cell suspension was centrifuged again at 400 \times g for 5 minutes, and the resulting pellet was suspended in PBS. The cells were then labeled in the presence of the ROCK inhibitor Y-27632 (10 μ mol/L; Miltenyi Biotec) with allophycocyanin (APC)-conjugated rat monoclonal antibodies to mouse EpCAM (#118214; Biolegend, San Diego, CA, USA) and FITC-conjugated rat monoclonal antibodies to mouse CD45 and CD31 (#102108 and #102406, respectively, Biolegend) for FACS with a MoFlo XDP Cell Sorter (Beckman Coulter). The EpCAM⁺CD45⁻CD31⁻ fraction was isolated as BECs.

2.3 | 3D culture of BECs as organoids

BECs were suspended in a Matrigel growth factor-reduced basement membrane matrix (Corning) and seeded on cell culture inserts (0.4 μ m, Corning) placed in the wells of a 24-well plate (Corning). After the Matrigel had solidified, expansion medium (EM) was added to each well outside of the insert. EM consisted of DMEM-F12 supplemented with recombinant human hepatocyte growth factor (50 ng/mL, Biolegend), recombinant human epidermal growth factor (50 ng/mL; Pepro Tech), recombinant human fibroblast growth factor 10 (100 ng/mL, Biolegend), nicotinamide (10 mmol/L, Sigma-Aldrich), recombinant human R-spondin-1 (0.5 μ g/mL, Miltenyi Biotec), B27 supplement without vitamin A (Life Technologies), and Y-27632 (10 μ mol/L). At 1 week after seeding, organoids were removed from the Matrigel for expansion of the cell culture. The Matrigel was mechanically dissociated into small fragments and incubated for 5 minutes at 37°C with TrypLE solution. The cell suspension was filtered with a 40- μ m nylon cell strainer, and the filtrate was centrifuged at 400 \times g for 5 minutes. The cells in the pellet were counted, suspended in fresh Matrigel, and cultured as organoids.

2.4 | Retroviral plasmids and retrovirus infection

The full-length human KRAS(G12V) cDNA was amplified by PCR from the plasmid pGCDN-KRAS^{G12V}-IRES-huKO²⁸ with the primers KRAS^{G12V}-sense (5'-CGGGATCCATGACTGAATATAAACTTGTGGTATTGGAGC-3', BamHI site underlined) and KRAS^{G12V}-antisense (5'-ATAAGAATGCGGCCGCTTACATAATTACACACTTTGTC-3' NotI site underlined). The PCR product was digested and ligated into the pMXs-IRES-GFP retroviral vector²⁹ to yield pMXs-IRES-GFP-KRAS(G12V). Plat-E packaging cells were transfected with pMXs-IRES-GFP-KRAS(G12V) or pMXs-IRES-GFP (control plasmid) with the use of the FugeneHD reagent (Promega), and the culture supernatants were subsequently collected, passed through a 0.45- μ m cellulose acetate filter (Iwaki), and centrifuged at 23 000 \times g for 4 hours at 4°C. The virus pellets were suspended in EM and added to BECs

in organoid culture. The GFP-positive infected cells were sorted by FACS with a MoFlo XDP Cell Sorter (Beckman Coulter).

2.5 | Single-cell cloning and culture

For clonogenic assays, GFP-positive cells were sorted from dissociated organoids on the basis of forward scatter and pulse width to discriminate single cells. Dead cells were labeled with propidium iodide, and cell doublets were excluded by gating based on forward scatter and pulse width. Single cells were captured with a MoFlo XDP Cell Sorter (Beckman Coulter), and the sorted cells were embedded in Matrigel, seeded in 96-well plates at a density of 1 cell per well, and maintained in 3D culture as described above.

2.6 | Implantation of KRAS(G12V)-expressing cells in recipient mice

KRAS(G12V)-expressing or control cells were injected as single-cell suspensions into WT C57BL/6J mice for intrahepatic, kidney subcapsular, or s.c. transplantation as described previously.¹⁴ The mice were anesthetized by i.p. injection of a combination of anesthetic agents (medetomidine [0.3 mg/kg], midazolam [4.0 mg/kg], and butorphanol [5.0 mg/kg]) before surgery. For intrahepatic injection, cells (5×10^4) suspended in 10 μ L of DMEM-F12 supplemented with 50% Matrigel growth factor-reduced matrix were transplanted in the liver parenchyma with the use of a 29G syringe (Terumo). The abdominal wall was then washed and closed with the use of absorbable sutures. For kidney subcapsular injection, cells (5×10^4) were implanted with a 29G syringe. For s.c. injection, cells (1×10^2 , 1×10^3 , 1×10^4 , or 5×10^4) were injected into the rear flank. The time course of tumor volume, Kaplan-Meier survival analysis, and the incidence of lung metastasis at 4 weeks for recipient mice were evaluated after s.c. injection of 5×10^4 cells.

2.7 | Establishment of tumor cells from tumor tissue

Primary tumors were dissected from recipient mice and subjected to mechanical and enzymatic dissociation as described for isolation of BECs. GFP-positive tumor cells were sorted from single-cell suspensions by FACS with a MoFlo XDP Cell Sorter (Beckman Coulter). For establishment of organoids, the GFP⁺ tumor cells were maintained in 3D culture as described above. For adherent culture, the sorted GFP⁺ tumor cells were suspended in EM and seeded in a 35-mm culture dish.

2.8 | Immunohistochemistry (IHC)

Tumor or normal tissue was fixed with 4% paraformaldehyde, embedded in paraffin, and sectioned, and the sections were then depleted of paraffin and stained with primary antibodies listed in

Table S1. Immune complexes were detected with biotinylated secondary antibodies and a Vectastain avidin and biotinylated horseradish peroxidase (HRP) macromolecular complex reagent and 3,3'-diaminobenzidine (Vector Laboratories).

2.9 | Immunohistofluorescence analysis

Immunohistofluorescence staining was performed with antibodies to GFP (biotinylated, #2912; Cell Signaling Technology), to CK19 (ab52625; Abcam), and to vimentin (#5741, Cell Signaling Technology). Immune complexes were detected with Alexa Fluor 594-conjugated goat antibodies to rabbit IgG or streptavidin- and Alexa Fluor 488-conjugated goat antibodies to biotin, and nuclei were stained with Hoechst 33342 (Sigma-Aldrich). Tissue sections were viewed with a Bioevo BZ-9000 fluorescence microscope (Keyence).

2.10 | Immunoblot analysis

Cells were lysed with SDS sample buffer (2% SDS, 10% glycerol, 50 mmol/L Tris-HCl [pH 6.8]) containing 1 mol/L DTT for fractionation by SDS-PAGE. The separated proteins were transferred to a PVDF membrane and exposed to primary antibodies listed in Table S1. Immune complexes were detected with HRP-conjugated secondary antibodies and ECL reagents (Chemi-Lumi One L; Nacalai Tesque).

2.11 | Flow cytometric analysis

Cultured cells were dissociated by exposure to cell dissociation buffer (Thermo Fisher Scientific), and the resulting single-cell suspensions were incubated with antibodies for 30 minutes at 4°C. The cells were labeled with antibodies listed in Table S2. Apoptotic cells were excluded during flow cytometric analysis by elimination of cells positive for staining with propidium iodide. Flow cytometry was performed with a FACSCalibur instrument (BD Biosciences), and data were analyzed with FlowJo software (FlowJo).

2.12 | RT and real-time PCR analysis

RT and real-time PCR analysis was performed as previously described.³⁰ The amount of each target mRNA was normalized by that of *Gapdh* mRNA. The primer sequences are listed in Table S3.

2.13 | Microarray analysis

Total RNA was extracted from organoids with the use of an RNeasy Mini Kit (Qiagen). The quality of the RNA was assessed with an Agilent 2100 Bioanalyzer (Agilent Technologies). Cy3-labeled cRNA probes were synthesized from the total RNA with the use of a Low Input Quick Amp Labeling Kit (Agilent Technologies) and were subjected to hybridization with a SurePrint G3 Mouse GE v2 8 × 60 K microarray (Agilent Technologies). Fluorescence images were visualized with an Agilent microarray scanner G2505C. The raw data for each spot were normalized by subtraction of the mean background signal intensity determined from the intensities of all blank spots with 95% confidence intervals and were analyzed with GeneSpring GX software (Tomy Digital Biology). Relative expression level was calculated by comparison of the signal intensities of valid spots throughout the microarray. The Spotfire Decision Site for Functional Genomics software package (TIBCO Software) was used for visualization of microarray data. Functional analysis was performed using the DAVID Bioinformatics Resources 6.8 (<http://david.abcc.ncifcrf.gov>). The probe IDs and data are listed in Tables S4 and S5, respectively. The microarray data are available in the Gene Expression Omnibus (GEO) database under the accession number GSE151442.

2.14 | Gene Set Enrichment Analysis (GSEA)

GSEA was performed with version 3.1 of the molecular signature database and the HALLMARK_EPITHELIAL_MESENCHYMAL_TRANSITION gene set.

2.15 | Statistical analysis

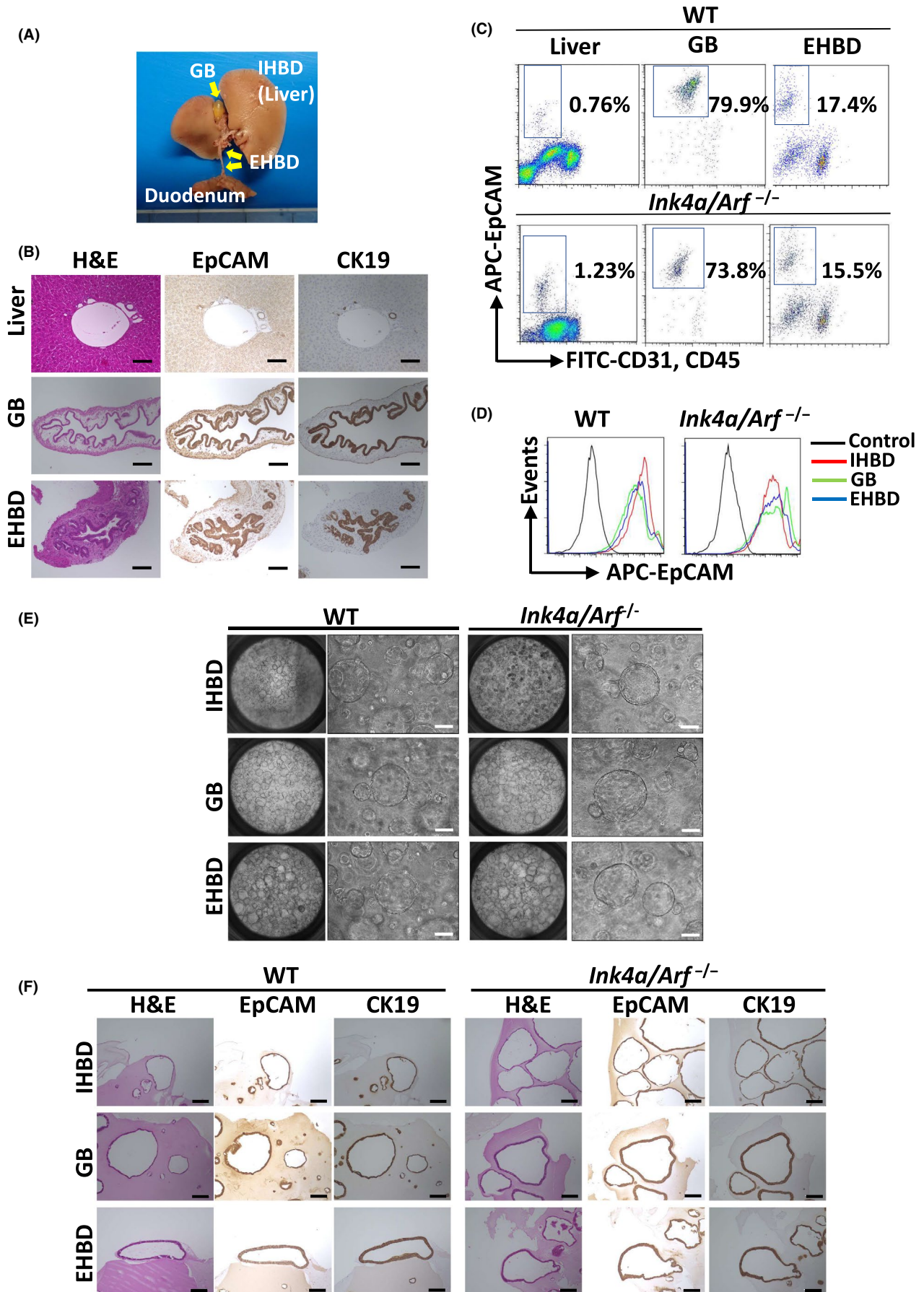
Data (means + SD) were compared using Student paired *t* test. A *P* value of < .05 was considered statistically significant.

3 | RESULTS

3.1 | Isolation and organoid culture of mouse BECs

IHC analysis of mouse liver (IHBD), GB, and EHBD confirmed that the corresponding BECs express EpCAM and CK19 (Figure 1A,B).

FIGURE 1 Isolation and organoid culture of mouse biliary epithelial cells (BECs). A, Representative gross morphology of the mouse liver, gall bladder (GB), extrahepatic bile duct (EHBD), and duodenum. The intrahepatic bile duct (IHBD) is located within the liver. B, H&E staining as well as IHC of EpCAM and CK19 in the mouse biliary tract (IHBD, GB, and EHBD). Scale bars, 100 μm. C, FACS of EpCAM⁺CD31⁻CD45⁻ cells from single-cell digests of the liver (IHBD), GB, and EHBD of WT and *Ink4a/Arf*^{-/-} mice. D, Organoids formed by cells isolated as in (C) were disrupted and subjected to flow cytometric analysis of EpCAM. Control represents staining with control IgG. E, Bright-field images (low and high magnification) of organoid cultures of BECs from WT and *Ink4a/Arf*^{-/-} mice. Scale bars, 100 μm. F, H&E staining and IHC of EpCAM and CK19 for BEC organoids of WT and *Ink4a/Arf*^{-/-} mice. Scale bars, 100 μm



We isolated EpCAM⁺CD31⁻CD45⁻ cells from the liver (IHBD), GB, and EHBD of both WT and *Ink4a/Arf*^{-/-} mice as BECs by FACS (Figure 1C). The population of EpCAM-positive BECs in the liver was small (0.76% and 1.23% in WT and *Ink4a/Arf*^{-/-} mice, respectively), given that most cells in the liver are hepatocytes. Single-cell suspensions of each type of BEC (IHBD, GB, and EHBD) were then suspended in Matrigel and subjected to organoid culture. EpCAM-positive cells were enriched after serial passage of BECs from both WT and *Ink4a/Arf*^{-/-} mice (Figure 1D). Flow cytometry revealed that EpCAM-positive cells constituted 98.05% of IHBD cells, 94.28% of GB cells, and 96.38% of EHBD cells in organoids derived from WT mice as well as 95.39%, 90.19%, and 92.73% of those, respectively, in organoids derived from *Ink4a/Arf*^{-/-} mice. Organoid structures were also maintained or restored after serial passage of BECs from both WT and *Ink4a/Arf*^{-/-} mice (Figure 1E). The morphology of BEC organoids was similar for both WT and *Ink4a/Arf*^{-/-} mice and did not change with serial passage. IHC analysis revealed that each type of organoid was composed of CK19- and EpCAM-positive cells (Figure 1F).

3.2 | Establishment of mouse BEC organoids expressing KRAS(G12V)

We next infected the organoid cultures for each type of BEC from WT and *Ink4a/Arf*^{-/-} mice either with a retrovirus encoding the oncogenic mutant KRAS(G12V)-GFP or with a control virus encoding GFP alone. Each type of WT BEC infected with the control virus was amenable to serial passage in culture. However, those infected with the virus for KRAS(G12V)-GFP did not proliferate, possibly as a result of oncogene-induced senescence dependent on *Ink4a/Arf*. We therefore used *Ink4a/Arf*^{-/-} BECs to develop our BTC models. The infected cells were isolated by FACS on the basis of their expression of GFP (Figure 2A) and were subjected to further organoid culture (Figure 2B). We have been able to maintain these organoids stably in culture for multiple passages. The organoids formed by *Ink4a/Arf*^{-/-} BECs infected with the control virus resembled those formed by noninfected cells, whereas those formed by the corresponding cells infected with the KRAS(G12V)-GFP virus manifested structural and cellular

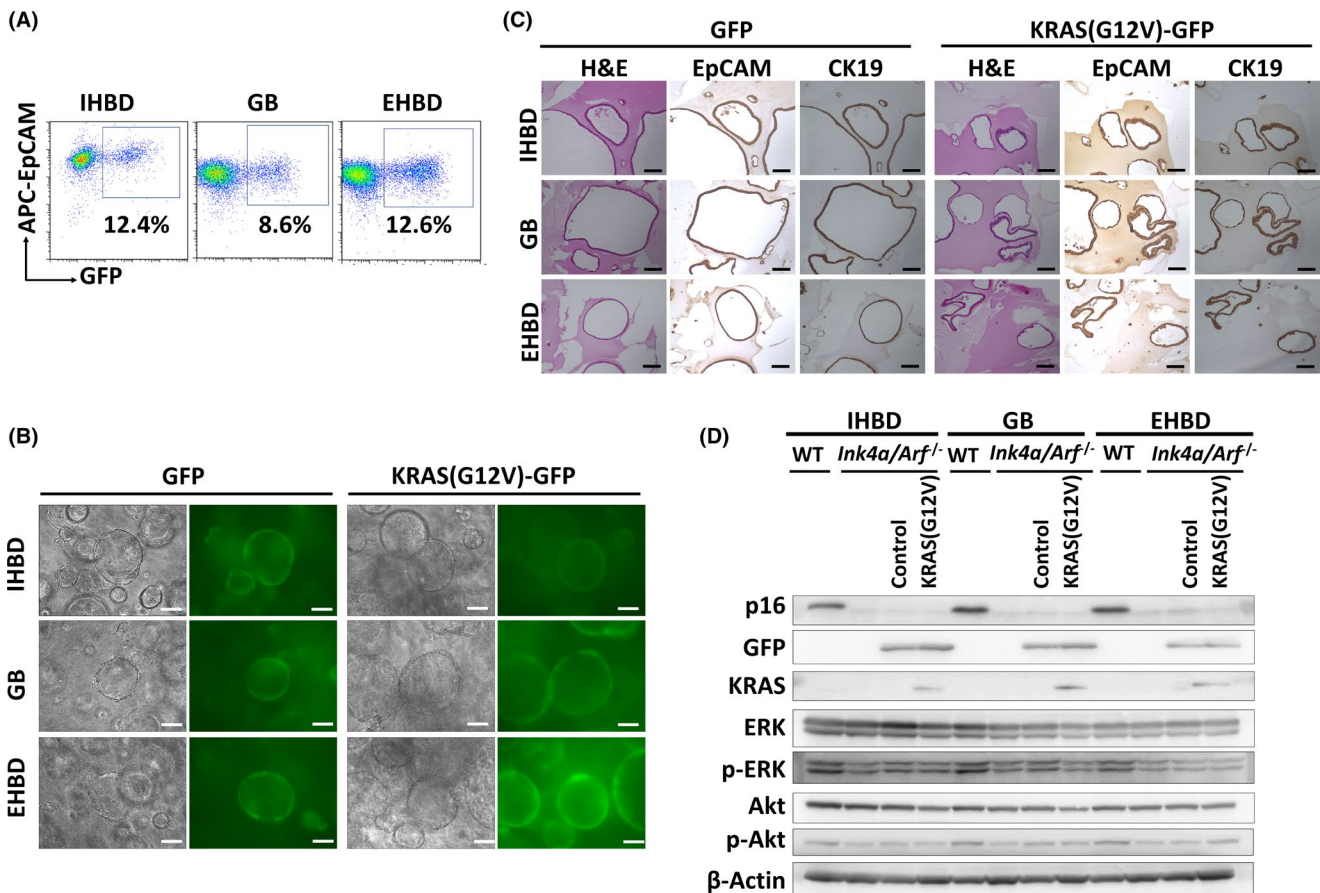


FIGURE 2 Establishment of mouse biliary epithelial cells (BECs) organoids expressing KRAS(G12V). A, Representative dot plots for flow cytometric analysis of GFP expression in BECs from *Ink4a/Arf*^{-/-} mice infected with a retrovirus encoding KRAS(G12V) and GFP. B, Bright-field and fluorescence images of organoid cultures of *Ink4a/Arf*^{-/-} BECs infected with retroviruses encoding GFP alone or both KRAS(G12V) and GFP. Scale bars, 100 μm. C, H&E staining and IHC for EpCAM and CK19 in *Ink4a/Arf*^{-/-} BEC organoids infected with GFP (control) or KRAS(G12V)-GFP viruses. Scale bars, 100 μm. D, Immunoblot analysis of p16, GFP, and KRAS as well as of total and phosphorylated (p-) forms of ERK and Akt in WT BECs and in *Ink4a/Arf*^{-/-} BECs infected (or not) with GFP (control) or KRAS(G12V)-GFP viruses. β-Actin was examined as a loading control

atypia, with regions showing the formation of multilayered cystic structures (Figure 2C). Immunoblot analysis revealed the expression of p16 in WT BECs, of GFP in *Ink4a/Arf*^{-/-} BECs infected with the control or KRAS(G12V)-GFP viruses, and of KRAS in *Ink4a/Arf*^{-/-} BECs infected with the KRAS(G12V)-GFP virus (Figure 2D). Immunoblot analysis also showed that the extent of ERK or Akt phosphorylation was not substantially affected by expression of KRAS(G12V). Microarray analysis revealed that the expression of 205 genes was increased >2-fold in *Ink4a/Arf*^{-/-} BECs infected with the KRAS(G12V)-GFP virus compared with those infected with the control virus, but gene ontology analysis did not detect significant changes for any functional category among these genes (data not shown).

3.3 | Tumor formation by KRAS(G12V)-expressing BECs in syngeneic mice

To determine whether KRAS(G12V)-expressing BECs from *Ink4a/Arf*^{-/-} mice are able to function as TICs, we implanted single-cell suspensions in immunocompetent syngeneic mice. The cells derived from the IHBD, GB, or EHBD formed lethal metastatic adenocarcinomas after intrahepatic, s.c., or renal subcapsular transplantation (Figure 3A-C). The phosphorylation of ERK was detected in the developed tumors (Figure 3A), suggesting that ERK signaling was activated by KRAS(G12V) and was associated with tumorigenesis. Given that ERK phosphorylation was not induced by KRAS(G12V) in the corresponding BECs in culture, the

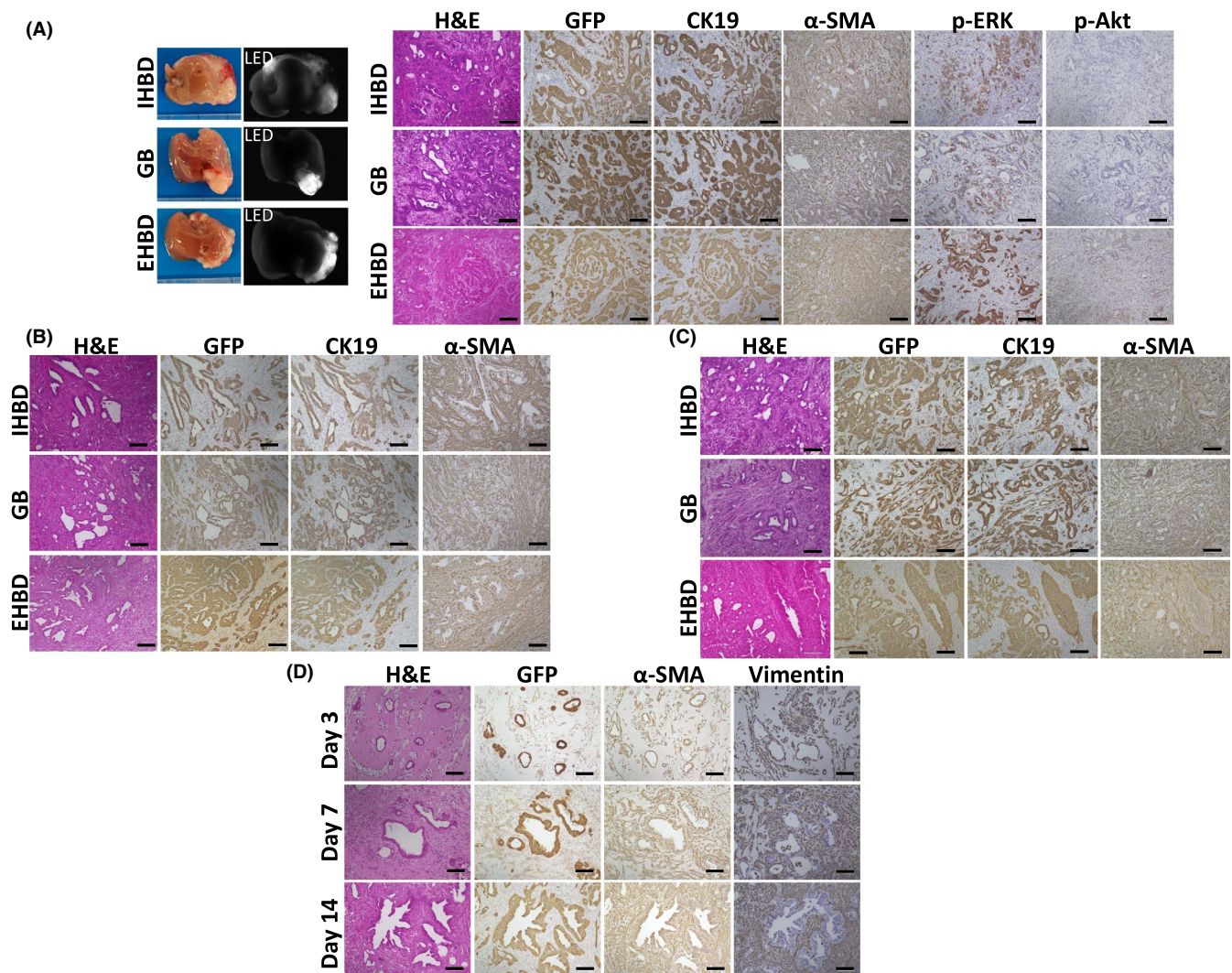


FIGURE 3 Tumor formation by KRAS(G12V)-expressing *Ink4a/Arf*^{-/-} biliary epithelial cells (BECs) in WT C57BL/6J mice. A, Macroscopic and microscopic appearance of tumors formed 4 wk after intrahepatic injection of KRAS(G12V)-expressing *Ink4a/Arf*^{-/-} IHBD-, GB-, or EHBD-derived BECs (5×10^4 cells) in syngeneic WT mice. The light-emitting diode (LED) images reveal GFP fluorescence. For microscopic analysis, tumor sections were subjected to H&E staining as well as to IHC of GFP, CK19, α-SMA, and phosphorylated (p-) forms of ERK and Akt. Scale bars, 100 μm. B, C, H&E staining and IHC of GFP, CK19, and α-SMA in tumors formed 4 wk after injection of KRAS(G12V)-expressing *Ink4a/Arf*^{-/-} BECs (5×10^4 cells) either s.c. (B) or below the kidney capsule (C) in syngeneic WT mice. Scale bars, 100 μm. D, H&E staining and IHC of GFP, α-SMA, and vimentin in tumors formed 3, 7, or 14 d after s.c. injection of KRAS(G12V)-expressing *Ink4a/Arf*^{-/-} IHBD cells (1×10^4 cells) in syngeneic WT mice. Scale bars, 100 μm

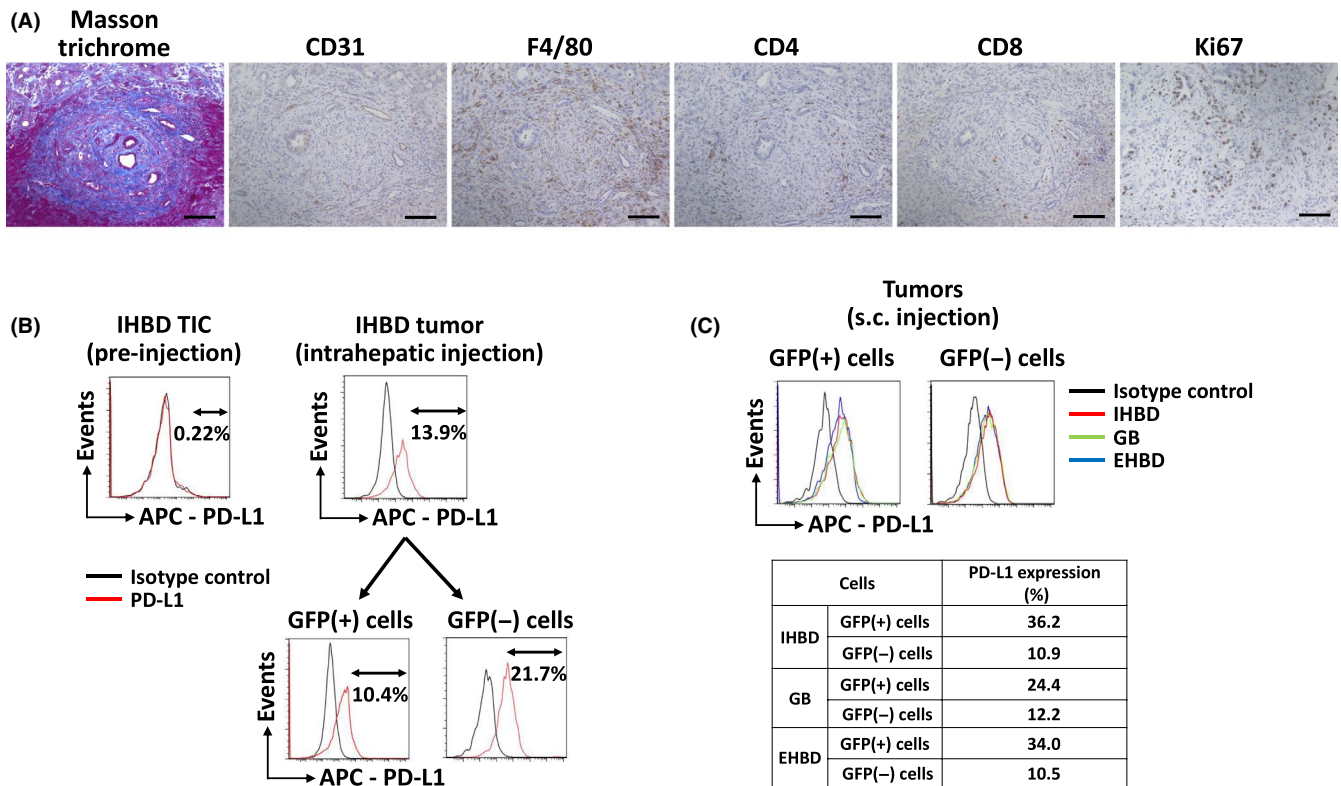


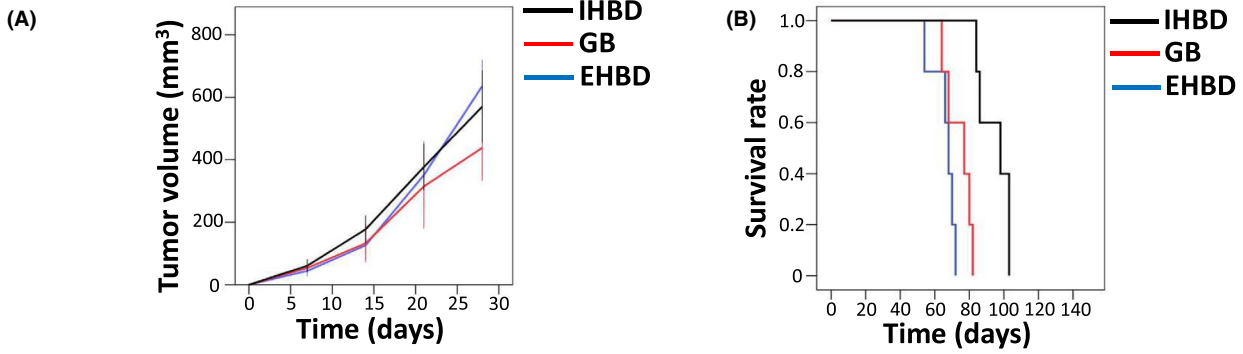
FIGURE 4 Microenvironments in tumors formed by KRAS(G12V)-expressing *Ink4a/Arf*^{-/-} biliary epithelial cells (BECs) in WT C57BL/6J mice. A, Masson trichrome staining as well as IHC of CD31, F4/80, CD4, CD8, and the cell proliferation marker Ki67 in tumors formed 4 wk after intrahepatic injection of KRAS(G12V)-expressing *Ink4a/Arf*^{-/-} intrahepatic bile duct (IHBD)-derived BECs (5×10^4 cells) in WT C57BL/6J mice. Scale bars, 100 μ m. B, Flow cytometric analysis of PD-L1 expression in IHBD tumor-initiating cells (TICs) before the inoculation (IHBD TIC) and in tumor-derived cells, which were isolated 4 wk after intrahepatic injection of the IHBD TICs (IHBD tumor). These cells were incubated with APC-conjugated rat monoclonal antibodies to mouse PD-L1 (red line). APC-conjugated rat IgG was used as isotype control antibody (black line). The expression of PD-L1 in GFP-positive tumor cells and in GFP-negative stromal cells is shown in lower panels. C, Flow cytometric analysis of PD-L1 expression in cells derived from tumors isolated 4 wk after s.c. injection of IHBD, gallbladder (GB), or extrahepatic bile duct (EHBD) TICs (5×10^4 cells). The cells derived from IHBD, GB, or EHBD tumors were incubated with APC-conjugated rat monoclonal antibodies to mouse PD-L1 (red, green, or blue line, respectively). The cells derived from IHBD tumors were incubated with isotype control antibody (APC-conjugated rat IgG, black line). The percentages of GFP-positive tumor cells and GFP-negative stromal cells expressing PD-L1 are also shown

activation of ERK signaling downstream of KRAS(G12V) in the tumors was likely either dependent on the tumor microenvironment or due to the selection of cells with activated ERK signaling. The tumors included differentiated components that expressed the epithelial cell marker CK19 (Figures 3A-C and S1). They also included stromal cell components that expressed α -smooth muscle actin (α -SMA), showing a pronounced desmoplastic reaction (Figure 3A-C). These results thus indicated that we had established BTC (IHCC, GC, or EHCC)-initiating cells, and that these cells formed tumors with features of human desmoplastic BTC.

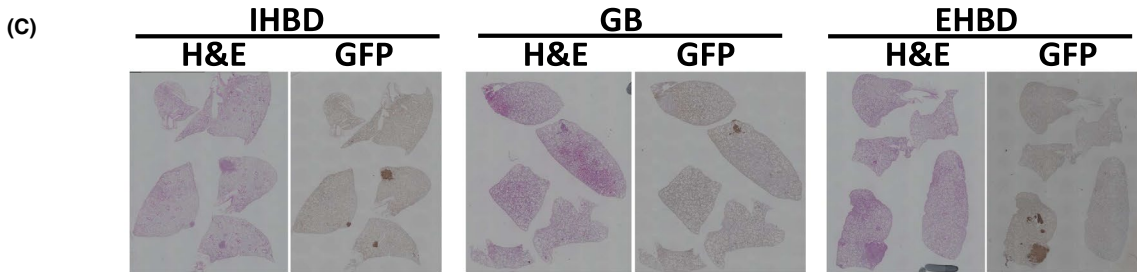
We further examined tumor histology at 3, 7, and 14 days after s.c. cell transplantation. At 3 days, GFP-positive tumor cells had expanded into bile duct epithelium-like structures without stromal components. At 7 days, α -SMA-positive fibroblasts had been recruited around the cystic structures. Infiltration of tumor cells accompanied by marked recruitment of α -SMA-positive cells had resulted in mass formation after 2 weeks (Figure 3D).

A major advantage of syngeneic mice as recipients is that tumors are able to grow in the setting of intact immunity. To characterize further the tumor microenvironment including immune cells for the

FIGURE 5 High tumorigenic and metastatic capacity of KRAS(G12V)-expressing *Ink4a/Arf*^{-/-} biliary epithelial cells (BECs). A, Time course for the volume of tumors formed after s.c. injection of KRAS(G12V)-expressing *Ink4a/Arf*^{-/-} BECs (5×10^4 cells) in syngeneic WT mice ($n = 5$ for each group). Data are means \pm SD. B, Kaplan-Meier survival analysis for the mice in (A). C, Incidence of initial tumor formation and lung metastasis for the mice in (A). H&E staining and IHC for GFP in lung metastatic lesions formed 4 wk after s.c. cell injection are also shown. D, Incidence of initial tumor formation in mice injected s.c. with various numbers of *Ink4a/Arf*^{-/-} BECs expressing either GFP alone or both KRAS(G12V) and GFP. E, Bright-field (low and high magnification) and fluorescence images of organoids formed by individual KRAS(G12V)-expressing *Ink4a/Arf*^{-/-} IHBD cells after single-cell cloning. Scale bars, 100 μ m. F, H&E staining of tumors formed 4 wk after s.c. injection of syngeneic WT mice with the single-cell clones (5×10^4 cells) derived from organoid culture shown in E. Scale bars, 100 μ m

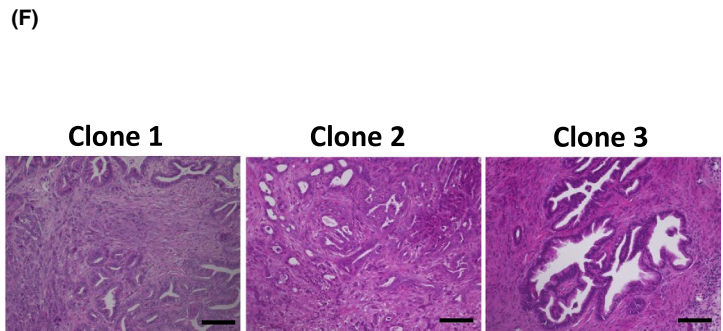
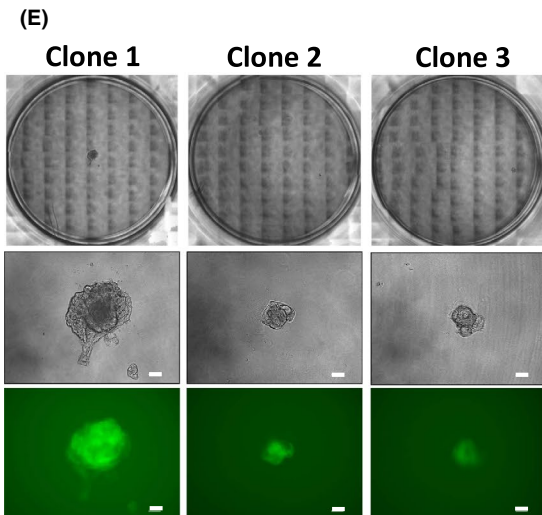


KRAS(G12V)-expressing BEC type	Grafted tumor	Lung metastasis
IHBD	5/5 (100%)	5/5 (100%)
GB	5/5 (100%)	5/5 (100%)
EHBD	5/5 (100%)	5/5 (100%)



(D)

Cell type	Cell number per injection site		
	1×10^4	1×10^3	1×10^2
IHBD (GFP)	0/6 (0%)	-	-
GB (GFP)	0/6 (0%)	-	-
EHBD (GFP)	0/6 (0%)	-	-
IHBD [KRAS(G12V)]	6/6 (100%)	6/6 (100%)	5/6 (83%)
GB [KRAS(G12V)]	6/6 (100%)	6/6 (100%)	5/6 (83%)
EHBD [KRAS(G12V)]	6/6 (100%)	6/6 (100%)	6/6 (100%)



BTC tumors, we performed IHC analysis of CD4, CD8, F4/80, and CD31. CD4⁺ T cells, CD8⁺ T cells, F4/80⁺ macrophages, and CD31⁺ endothelial cells were detected mostly in desmoplastic areas where tumor cells were surrounded by stromal cells and ECM (Figures 4A and S2). The tumors thus comprised both tumor cells and various microenvironmental components including fibroblasts, ECM, blood vessels, macrophages, and T cells. We also performed flow cytometric analysis of programmed cell death–ligand 1 (PD-L1) expression in cells isolated from the developed tumors. Although PD-L1 was expressed at only a low level in BTC cells before transplantation, it was highly expressed in both GFP–positive tumor cells and GFP–negative microenvironmental cells isolated from recipient mice (Figure 4B,C). These data thus indicated the presence of an immunosuppressive tumor microenvironment in our model mice.

3.4 | High tumorigenic and metastatic capacity of KRAS(G12V)–expressing BECs

We next examined the kinetics of tumor growth and its effects on the survival of immunocompetent syngeneic mice with s.c. implants of KRAS(G12V)–expressing *Ink4a/Arf*^{−/−} BECs. The tumors grew rapidly (Figure 5A) and were highly invasive, with a median survival time for the host animals of ~60 to 100 days (IHBD, 98 days; GB, 77 days; EHBD, 68 days) (Figure 5B). The frequency of lung metastasis was 100% for tumors formed by each type of BEC (Figure 5C). Limiting dilution analysis revealed that, in contrast with BECs expressing only GFP, which did not form tumors, those expressing KRAS(G12V) had a high tumor–initiating ability, with as few as 100 KRAS(G12V)–expressing BECs being sufficient for tumor formation (Figure 5D).

Single-cell cloning of BTC–initiating cells showed that some clones of KRAS(G12V)–expressing *Ink4a/Arf*^{−/−} BECs from the IHBD were able to form organoids in 3D culture (Figure 5E). Each such single-cell clone formed tumors with an adenocarcinoma histology and pronounced desmoplastic reaction in immunocompetent mice (Figure 5F), indicating that the implanted cells were able to function as TICs.

3.5 | CSC properties of cells derived from primary tumors are supported by subsequent organoid culture but not by adherent culture

We next isolated GFP–positive tumor cells from primary tumors formed as a result of s.c. transplantation of BTC–initiating cells

(Figure 6A). We established organoids in 3D culture from these cells and found that the organoids manifested structural and cellular atypia (Figure 6B) similar to that of primary organoids formed by KRAS(G12V)–expressing *Ink4a/Arf*^{−/−} BECs (Figure 2C). We performed a serial transplantation assay to examine whether these tumor–derived cells could form secondary s.c. tumors. The cells formed adenocarcinoma showing a desmoplastic reaction (Figure 6C), with the secondary tumors being pathologically similar to the corresponding primary tumors (Figure 3A–C), suggesting that these established cells possess CSC properties. Similar to the primary TICs, as few as 100 of the secondary organoid–derived cells was sufficient for formation of s.c. tumors (Figure 6D).

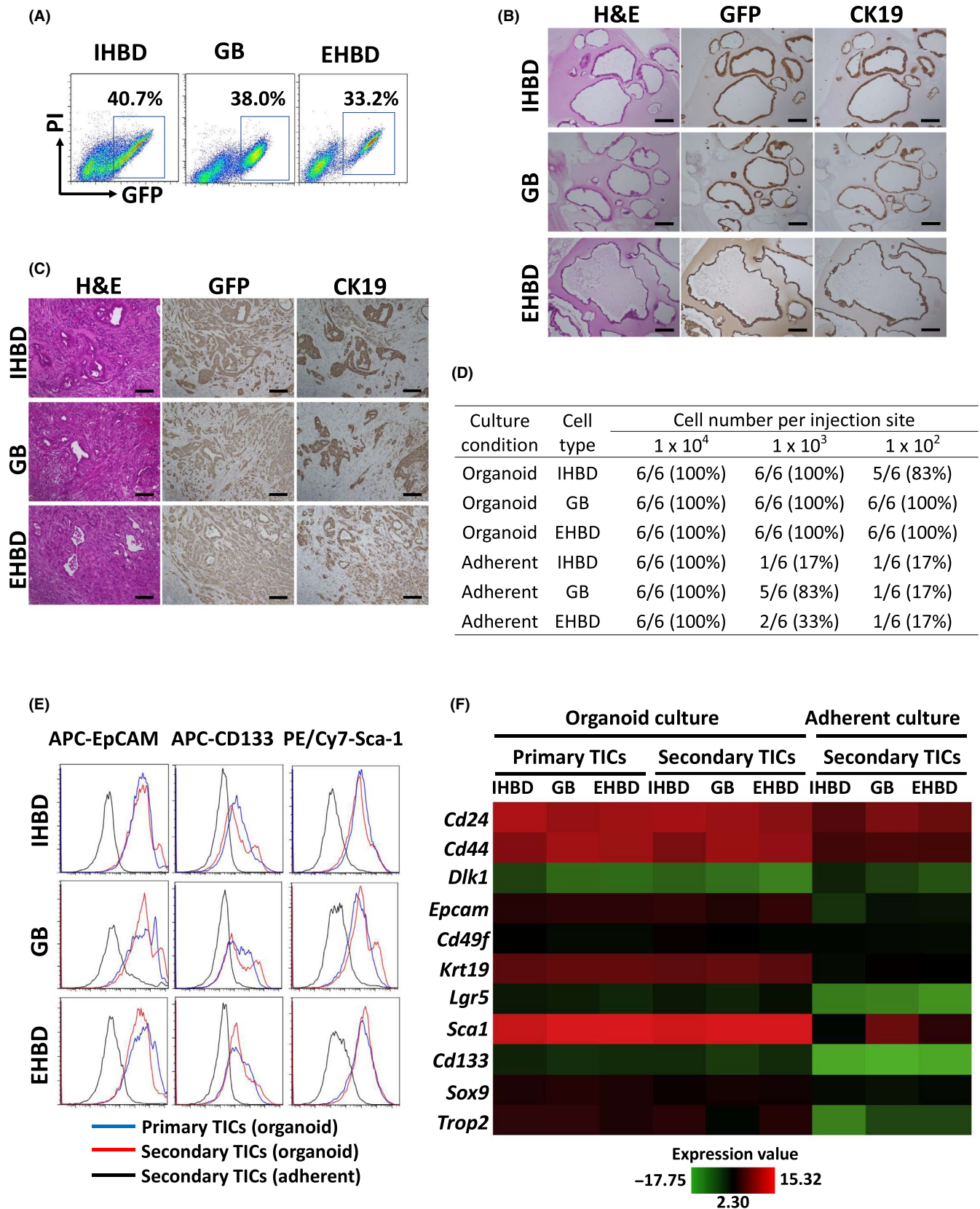
We also established adherent cultures of cells derived from the same primary tumors as those that gave rise to the secondary organoids used for these experiments. The cells maintained in adherent culture were spindle shaped (Figure S3) and manifested a lower tumor–initiating ability compared with the cells derived from secondary organoids (Figure 6D).

We examined the expression of EpCAM, CD133, and Sca-1 proteins in both primary and secondary TICs, given that these proteins are thought to be stem–progenitor cell markers in BTC.^{26,31} Flow cytometry revealed that the proportion of cells positive for each of these marker proteins was much higher for the primary or secondary cells maintained in organoid culture compared with the secondary cells maintained in adherent culture (Figure 6E). Microarray analysis also revealed that expression of biliary tract CSC marker genes in primary or secondary TICs was maintained by organoid culture but not by adherent culture (Figure 6F). Collectively, these findings suggested that adherent culture attenuated the CSC nature of organoid cells.

3.6 | EMT-related gene expression in BTC models

In addition to the loss of expression of BTC stem cell markers, GSEA of the microarray data revealed that the EMT gene set was significantly enriched for the secondary TICs maintained under the adherent condition relative to those maintained in organoid culture (Figure 7A). Immunoblot analysis also showed that expression of the epithelial cell markers EpCAM and E-cadherin was attenuated, whereas that of the mesenchymal cell marker vimentin was induced, in the secondary TICs maintained in adherent culture compared with those maintained in organoid culture (Figure 7B). We further evaluated 3- and 6-week-old primary tumors formed from a single-cell clone (IHBD clone 1). At

FIGURE 6 Cancer stem cell (CSC) properties are supported by organoid culture but not by adherent culture. A, Flow cytometric analysis for GFP expression and propidium iodide (PI) staining in cells derived from primary tumors formed 6 wk after s.c. injection of KRAS(G12V)–expressing *Ink4a/Arf*^{−/−} biliary epithelial cells (BECs) (5×10^4 cells) in syngeneic WT mice. The percentages of GFP⁺PI[−] cells for each primary tumor are shown. B, H&E staining and IHC of GFP and CK19 for secondary organoids derived from GFP–positive cells isolated from tumors as in (A). Scale bars, 100 μ m. C, H&E staining and IHC of GFP and CK19 for tumors formed 4 wk after s.c. transplantation of secondary TICs (5×10^4) that had been maintained in organoid culture as in (B). Scale bars, 100 μ m. D, Incidence of tumor formation in WT C57BL/6J mice injected s.c. with the indicated numbers of secondary TICs that had been maintained in organoid or adherent culture. E, Flow cytometric analysis of EpCAM, CD133, and Sca-1 expression in primary and secondary TICs maintained in organoid or adherent culture. F, Heat map of biliary tract CSC marker gene expression as determined by microarray analysis of IHBD, GB, and EHBD cells as in (E).



the early stage of tumor development, most GFP-positive tumor cells were epithelial cells, whereas at the late stage the GFP-positive tumor cells comprised both epithelial and mesenchymal-like cells (Figure 7C,D). Desmoplastic reactions were also more pronounced at

the late stage of tumor development. Given that the adherent culture condition resulted in a loss of both epithelial stem cell properties and tumorigenic activity, our data showed the importance of organoid culture to sustain epithelial stem cell properties as well as demonstrated

a relation between epithelial stem cell properties and tumorigenesis. We next implanted the corresponding secondary TICs that had been maintained under adherent or organoid culture conditions in new recipient WT mice and examined the phenotypes of the resulting tumors (Figure 7E). Secondary TICs derived from 6-week-old primary tumors and maintained as organoids formed tumors comprised of epithelial tumor cells (cystic structures) and vimentin-positive mesenchymal-like tumor cells, whereas secondary TICs maintained in adherent culture formed tumors comprised of vimentin-positive mesenchymal-like tumor cells (Figure 7E).

3.7 | Expression of EMT transcription factor genes in adherent-cultured TICs

We implanted primary TICs derived from a single-cell clone (IHBD clone 1) into syngeneic WT mice, isolated the resulting s.c. tumors after 3 or 6 weeks, and then cultured the tumor cells under adherent or organoid conditions. The morphology of the tumor cells maintained under the adherent condition differed between those isolated at 3 weeks and those isolated at 6 weeks, with the latter cells manifesting a more prominent spindle shape (Figure S4). Immunoblot analysis revealed that the abundance of vimentin was increased and that of EpCAM decreased in the cells maintained in adherent culture relative to those maintained in organoid culture, with the amount of vimentin being increased to a greater extent in the adherent cells derived from the older primary tumors (Figure 8A). RT and real-time PCR analysis showed that expression of the EpCAM gene was also markedly decreased in cells maintained under the adherent condition (Figure 8B). We also examined the expression of genes for EMT-related transcription factors (EMT-TFs) including ZEB1, ZEB2, SNAIL1, SNAIL2, TWIST1, and TWIST2, all of which induce EMT by suppressing the expression of cell adhesion molecules.³² Significant up-regulation of *Zeb1*, *Zeb2*, *Snail1*, *Snail2*, *Twist1*, and *Twist2* mRNAs was apparent in the cells maintained in adherent culture, and, with the exception of *Twist1* mRNA, the extent of this up-regulation was greater in the cells derived from the older tumors (Figure 8B).

4 | DISCUSSION

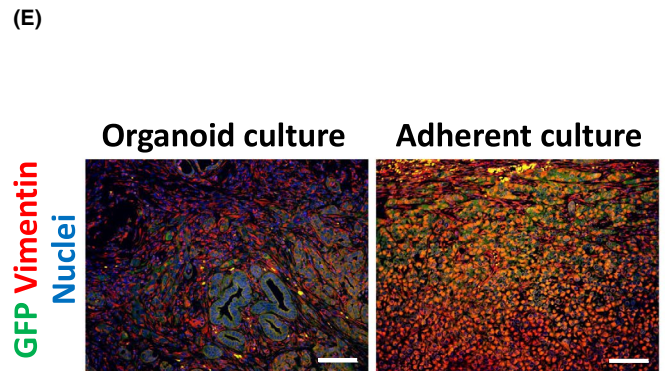
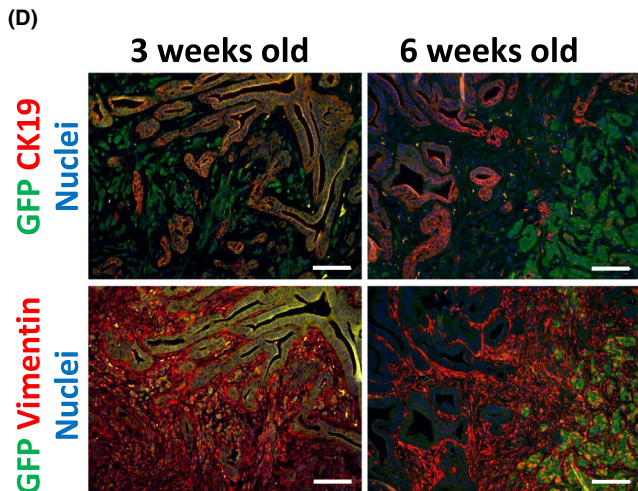
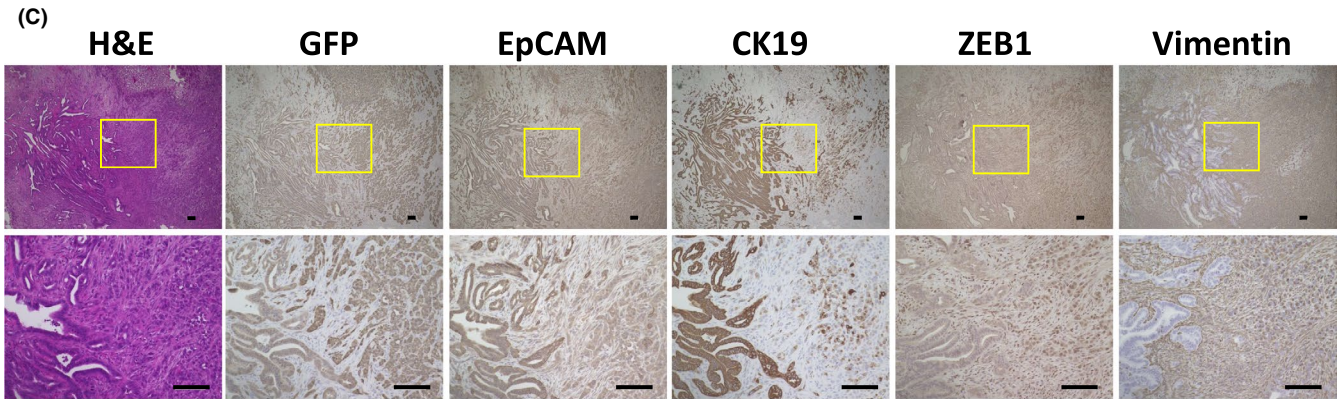
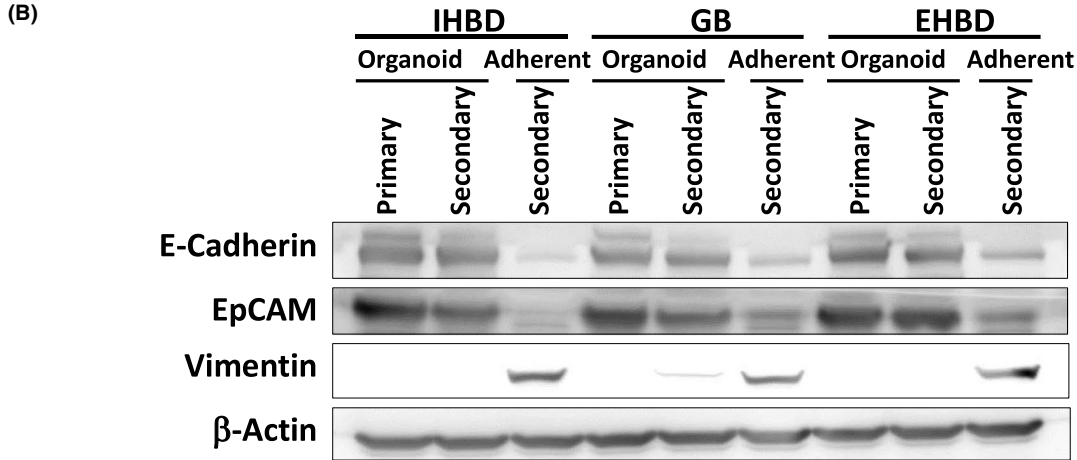
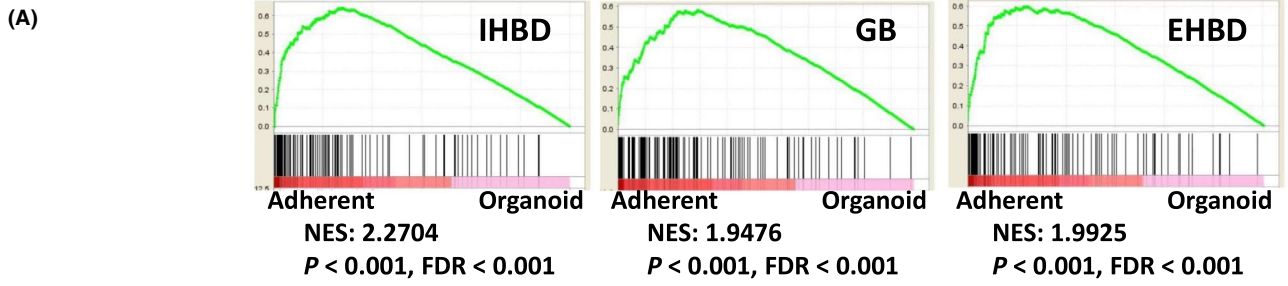
To provide insight into the molecular pathogenesis of BTC, we have here established BTC-initiating cells for IHCC, GC, and EHCC.

EpCAM-positive BECs isolated from the IHBD, GB, or EHBD of *Ink4a/Arf* knockout C57BL/6J mice were maintained as organoids in 3D culture and then infected with a retrovirus encoding KRAS(G12V). Transplantation of the BTC-initiating cells derived from the BEC-specific organoid cultures into syngeneic WT C57BL/6J mice gave rise to the formation of lethal metastatic adenocarcinomas with heterogeneous differentiated components and pronounced desmoplastic reactions.

The liver is composed mostly of 2 epithelial cell types: hepatocytes (EpCAM⁻) and cholangiocytes (EpCAM⁺ ductal cells). Normal EpCAM⁺ IHBD cells were previously shown to include liver stem cells, and organoids derived from these cells were found to undergo conversion to functional hepatocytes.²¹ Normal BECs have also been isolated from the GB, and the EpCAM⁺CD49f⁺ GB cells were shown to possess self-renewal ability and to undergo organotypic morphogenesis to form ductlike structures and cysts reminiscent of the primary GB.³³ In addition, EpCAM⁺ peribiliary glands, clusters of epithelial cells residing in the submucosal compartment of the EHBD, were found to link epithelial networks within the wall of the EHBD and might function as BEC stem cells.^{34,35} Similar to normal stem cells, we obtained cultures of KRAS(G12V)-expressing EpCAM⁺ BECs (IHBD, GB, and EHBD cells) as organoids in serum-free medium supplemented with growth factors. We established and enriched BTC-initiating cells with epithelial stem cell properties, and these TICs were found to be capable of serial syngeneic transplantation, with maintenance of high tumorigenic activity in organoid culture over a long period. In contrast, TICs maintained in adherent culture showed attenuation both of tumorigenic activity and of the expression of both epithelial and stem cell markers. Our data thus indicate that organoid culture is necessary for maintenance of epithelial cell characteristics, stemness, and tumorigenic activity in BTC-initiating cells.

Adult liver stem-progenitor cells are bipotent cells capable of differentiating into either hepatocytes or BECs (cholangiocytes). Cholangiocarcinoma within the liver is a tumor of the bile duct epithelium, but IHCC has been suggested to originate from differentiated hepatocytes via trans-differentiation in injured liver.^{36,37} Conversely, a cholangiocyte lineage-tracing system implicated BECs as a possible origin of IHCC.³⁸ In the present study, we established a mouse model for IHCC originating from EpCAM⁺ BECs. Given that cholangiocarcinoma is strongly associated with chronic biliary tract infection and inflammation,³⁹ we suggest that the fate of IHCC is dependent on the tissue microenvironment, including the recruitment

FIGURE 7 EMT-related gene expression in biliary tract cancer (BTC) models. A, GSEA of microarray data for the EMT gene set in secondary tumor-initiating cells (TICs) that had been maintained in adherent or organoid culture. NES, normalized enrichment score; FDR, false discovery rate. B, Immunoblot analysis of E-cadherin, EpCAM, and vimentin in whole lysates of cells as in Figure 6E. C, H&E staining as well as IHC of GFP, EpCAM, CK19, ZEB1, and vimentin in primary tumors formed by IHBD clone 1 (5×10^4 cells) at 6 wk after s.c. injection in syngeneic WT hosts. The boxed regions in the upper panels are shown at higher magnification in the lower panels. Scale bars, 100 μ m. D, Immunofluorescence analysis of GFP and either CK19 or vimentin in primary tumors formed by IHBD clone 1 (5×10^4 cells) at 3 or 6 wk after s.c. injection in syngeneic WT hosts. Nuclei were stained with Hoechst 33342 (blue). Scale bars, 100 μ m. E, Immunofluorescence analysis of GFP and vimentin in secondary tumors formed 4 wk after s.c. implantation in new recipients of IHBD clone 1 cells (5×10^4 cells) derived from 6-wk-old primary tumors as in (D) and then maintained in organoid or adherent culture for 4 wk before transplantation. Nuclei were stained with Hoechst 33342 (blue). Scale bars, 100 μ m



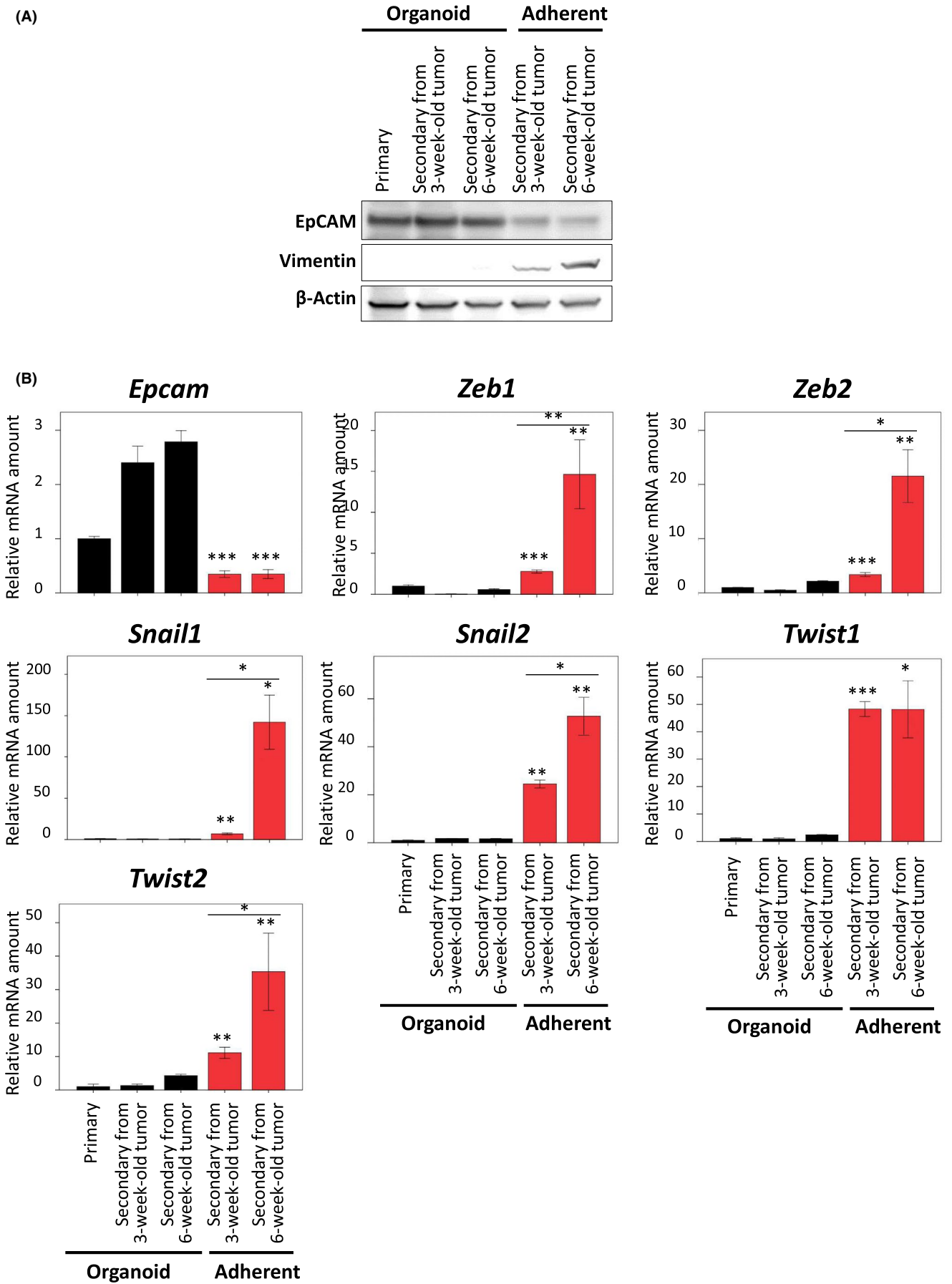


FIGURE 8 Expression of epithelial-mesenchymal transition (EMT)-related genes in primary and secondary tumor-initiating cells (TICs) from a single-cell clone (IHBD clone 1). A, Immunoblot analysis of EpCAM and vimentin in whole lysates of primary TICs maintained in organoid culture as well as of secondary TICs maintained in organoid or adherent culture. The secondary TICs were derived from tumors formed 3 or 6 wk after s.c. injection of KRAS(G12V)-expressing *Ink4a/Arf*^{-/-} IHBD clone 1 (5×10^4 cells) into syngeneic WT hosts. B, RT and real-time PCR analysis of *Epcam*, *Zeb1*, *Zeb2*, *Snail1*, *Snail2*, *Twist1*, and *Twist2* mRNAs in cells as in (A). The data were normalized by the amount of *Gapdh* mRNA, are expressed relative to the corresponding value for primary TICs, and are means \pm SD of triplicate experiments. * $P < .05$, ** $P < .01$, *** $P < .001$ vs primary TICs or for the indicated comparisons (Student paired t test)

of inflammatory cells and release of pro-inflammatory cytokines (such as interleukin-6 and transforming growth factor- β [TGF- β]) that promote the proliferation of cholangiocytes and fibroblasts.

In our models, BTCs arising from cells maintained in organoid culture consist of heterogeneous adenocarcinoma components containing epithelial-type and mesenchymal-type tumor cells and show a pronounced desmoplastic reaction. However, maintenance of TICs in adherent culture attenuated the expression of both epithelial and stem cell markers, whereas the expression of EMT-TFs and the mesenchymal cell marker vimentin was increased. Such cells had a lower tumorigenicity compared with the secondary BTC-initiating cells with CSC properties that were propagated by organoid culture. Furthermore, in contrast to tumors derived from organoid cells, there was no obvious desmoplastic reaction or infiltration of CD4⁺ or CD8⁺ T cells in tumors derived from adherent-cultured cells (Figure S5). Our results suggest that CSCs with EMT potential are more tumorigenic compared with cells that have become mesenchymal. Recent studies have indicated that EMT is associated with malignancy in various types of cancer, and activation of EMT signaling in cancer cells is thought to contribute to metastasis, recurrence, or therapeutic resistance.^{25,40} Wnt, TGF- β , Notch, Hedgehog, and Hippo signaling pathways play a role in the development of cholangiocarcinoma as well as in embryonic liver morphogenesis, and TGF- β , Wnt, and Notch promote EMT or the acquisition of mesenchymal features.⁴¹ EMT potential may therefore be a critical feature of cholangiocarcinoma. Indeed, loss of cell-to-cell adhesion and increased expression of EMT-TFs have been detected in human BTC specimens and are associated with a poor clinical outcome.^{42,43} However, cumulative changes in EMT-related markers, rather than changes in either epithelial or mesenchymal markers alone, should be taken into account in the prediction of clinical outcome. We therefore investigated the relation of *KRT19* (CK19 gene) and *ZEB1* mRNA abundance in primary tumors to the prognosis of patients with cholangiocarcinoma in the cBioPortal database (www.cbioportal.org). Analysis of 36 such patients revealed an association between high expression of both *KRT19* and *ZEB1* and poor survival, suggesting that intratumoral heterogeneity characterized by the presence of both epithelial-type and mesenchymal-type tumor cells may contribute to a poor clinical outcome.

Preclinical cancer models provide insight into the pathogenesis and treatment of cancer.^{44,45} To establish mouse models that recapitulate features of human malignant tumors, we have previously generated mice with various tumor types that are derived from iCSCs and consist of a hierarchy of heterogeneous tumor cells.²⁷ We have now established mouse BTC organoids and syngeneic mouse models of BTC by improving methods to sustain epithelial

stem cell characteristics. The tumors formed after transplantation of BTC-initiating cells derived from BTC organoids recapitulate the pathological features of human BTC (IHCC, GC, and EHCC) including a desmoplastic reaction and lung metastasis. The advantages of our mouse models include the facts that the high tumorigenesis efficiency (100%) and the characteristics of tumor growth in vivo are highly consistent, which allows detailed histopathologic analysis at different stages of tumor development. Furthermore, given that our models are based on syngeneic rather than immunodeficient mouse hosts, the tumor microenvironment, including antitumor immunity systems, is preserved, which allows the identification of interactions between tumor cells and host cells. In vitro and in vivo models based on human cholangiocarcinoma-derived organoids were recently developed for studies of the pathophysiology of primary tumors.^{46,47} Given that organoids reproduce the properties of primary tumors,⁴⁸⁻⁵¹ human BTC organoids and our mouse BTC models based on an organoid culture system are likely to prove valuable research tools for clarification of the mechanisms underlying BTC carcinogenesis.

Gene amplification for mutant *KRAS* has been detected in a substantial fraction of lung⁵² and prostate⁵³ cancers, and it is apparent in many cases of pancreatic cancer in The Cancer Genome Atlas (TCGA).⁵⁴ In addition, such cases have been found to be clinically aggressive. Although limited information is available for biliary carcinomas, a tumor with high expression of mutant *KRAS* as a result of gene amplification is present in the TCGA database (Figure S6). Furthermore, a previous study identified 2 of 182 cases of biliary tract cholangiocarcinoma in Taiwan as being positive for both *KRAS* mutation and gene amplification.⁵⁵ The BTC-initiating cells established in the present study by KRAS(G12V) overexpression possess CSC properties and therefore generate aggressive tumors characterized by a high tumorigenic activity and metastatic ability in mice.

In conclusion, we have established novel organoids and syngeneic mouse models of IHCC, GC, and EHCC based on KRAS activation and homozygous *Ink4a/Arf* deletion in corresponding EpCAM⁺ BECs. The tumors formed in these models recapitulate the histology of human BTC. Further studies with these organoids and animal models should provide a better understanding of CSCs for human BTC and contribute to the development of new therapeutic strategies for these malignancies.

ACKNOWLEDGMENTS

We thank R. Harigai, I. Ishimatsu, S. Hayashi, M. Sato, M. Kobori, S. Yumino, A. Sonoda, and other laboratory members for technical assistance, as well as Collaborative Research Resources, Keio University School of Medicine, for technical support. This study was

supported by Keio Gijuku Academic Development Funds (to YA); by Translational Research Network Program, Research on Applying Health Technology, and Research on Rare and Intractable Diseases grants from the Japan Agency for Medical Research and Development (to HS); and by Grants-in-Aid for Scientific Research from the Ministry of Education, Culture, Sports, Science, and Technology of Japan (KAKENHI 22130007 to HS, KAKENHI 20K08968 to YA).

DISCLOSURE

The authors declare no conflict of interest.

ORCID

Akiyoshi Kasuga  <https://orcid.org/0000-0002-2234-1135>

Eiji Sugihara  <https://orcid.org/0000-0002-3233-1045>

Yoshimi Arima  <https://orcid.org/0000-0002-2384-1406>

REFERENCES

- Jemal A, Bray F, Center MM, Ferlay J, Ward E, Forman D. Global cancer statistics. *CA Cancer J Clin*. 2011;61(2):69-90.
- Patel T. Worldwide trends in mortality from biliary tract malignancies. *BMC Cancer*. 2002;2:10.
- Valle J, Wasan H, Palmer DH, et al. Cisplatin plus gemcitabine versus gemcitabine for biliary tract cancer. *N Engl J Med*. 2010;362:1273-1281.
- Nakamura H, Arai Y, Totoki Y, et al. Genomic spectra of biliary tract cancer. *Nat Genet*. 2015;47:1003-1010.
- Tannapfel A, Benicke M, Katalinic A, et al. Frequency of p16(INK4A) alterations and K-ras mutations in intrahepatic cholangiocarcinoma of the liver. *Gut*. 2000;47:721-727.
- Sia D, Tovar V, Moeini A, Llovet JM. Intrahepatic cholangiocarcinoma: pathogenesis and rationale for molecular therapies. *Oncogene*. 2013;32:4861-4870.
- Xu X, Kobayashi S, Qiao W, et al. Induction of intrahepatic cholangiocellular carcinoma by liver-specific disruption of Smad4 and Pten in mice. *J Clin Invest*. 2006;116:1843-1852.
- O'Dell MR, Huang JL, Whitney-Miller CL, et al. Kras(G12D) and p53 mutation cause primary intrahepatic cholangiocarcinoma. *Can Res*. 2012;72:1557-1567.
- Nakagawa H, Suzuki N, Hirata Y, et al. Biliary epithelial injury-induced regenerative response by IL-33 promotes cholangiocarcinogenesis from peribiliary glands. *Proc Natl Acad Sci USA*. 2017;114:E3806-E3815.
- Ikenoue T, Terakado Y, Nakagawa H, et al. A novel mouse model of intrahepatic cholangiocarcinoma induced by liver-specific Kras activation and Pten deletion. *Sci Rep*. 2016;6:23899.
- Cristinziano G, Porru M, Lamberti D, et al. FGFR2 fusion protein-driven mouse models of intrahepatic cholangiocarcinoma unveil a necessary role for Erk signaling. *bioRxiv*. 2020. <https://doi.org/10.1101/2020.05.20.106104>
- Ochiai M, Yoshihara Y, Maru Y, et al. Kras-driven heterotopic tumor development from hepatobiliary organoids. *Carcinogenesis*. 2019;40:1142-1152. <https://doi.org/10.1093/carcin/bgz024>
- Saborowski A, Wolff K, Spielberg S, et al. Murine liver organoids as a genetically flexible system to study liver cancer in vivo and in vitro. *Hepatol Commun*. 2019;3:423-436.
- Erlangga Z, Wolff K, Poth T, et al. Potent antitumor activity of liposomal irinotecan in an organoid- and CRISPR-Cas9-based murine model of gallbladder cancer. *Cancers*. 2019;11(12):1904.
- Sato T, Vries RG, Snippert HJ, et al. Single Lgr5 stem cells build crypt-villus structures in vitro without a mesenchymal niche. *Nature*. 2009;459:262-265.
- Sato T, van Es JH, Snippert HJ, et al. Paneth cells constitute the niche for Lgr5 stem cells in intestinal crypts. *Nature*. 2011;469:415-418.
- Sato T, Stange DE, Ferrante M, et al. Long-term expansion of epithelial organoids from human colon, adenoma, adenocarcinoma, and Barrett's epithelium. *Gastroenterology*. 2011;141:1762-1772.
- Barker N, Huch M, Kujala P, et al. Lgr5(+ve) stem cells drive self-renewal in the stomach and build long-lived gastric units in vitro. *Cell Stem Cell*. 2010;6:25-36.
- Huch M, Dorrell C, Boj SF, et al. In vitro expansion of single Lgr5+ liver stem cells induced by Wnt-driven regeneration. *Nature*. 2013;494:247-250.
- Huch M, Bonfanti P, Boj SF, et al. Unlimited in vitro expansion of adult bi-potent pancreas progenitors through the Lgr5/R-spondin axis. *EMBO J*. 2013;32:2708-2721.
- Huch M, Gehart H, van Boxtel R, et al. Long-term culture of genome-stable bipotent stem cells from adult human liver. *Cell*. 2015;160:299-312.
- Itoh T, Miyajima A. Liver regeneration by stem/progenitor cells. *Hepatology*. 2014;59:1617-1626.
- Miyajima A, Tanaka M, Itoh T. Stem/progenitor cells in liver development, homeostasis, regeneration, and reprogramming. *Cell Stem Cell*. 2014;14:561-574.
- Schmelzer E, Zhang L, Bruce A, et al. Human hepatic stem cells from fetal and postnatal donors. *J Exp Med*. 2007;204:1973-1987.
- Sato R, Semba T, Saya H, Arima Y. Concise review: stem cells and epithelial-mesenchymal transition in cancer: biological implications and therapeutic targets. *Stem Cells*. 2016;34:1997-2007.
- Yamashita T, Wang XW. Cancer stem cells in the development of liver cancer. *J Clin Invest*. 2013;123:1911-1918.
- Sugihara E, Saya H. Complexity of cancer stem cells. *Int J Cancer*. 2013;132:1249-1259.
- Tamase A, Muraguchi T, Naka K, et al. Identification of tumor-initiating cells in a highly aggressive brain tumor using promoter activity of nucleostemin. *Proc Natl Acad Sci USA*. 2009;106:17163-17168.
- Kitamura T, Koshino Y, Shibata F, et al. Retrovirus-mediated gene transfer and expression cloning: powerful tools in functional genomics. *Exp Hematol*. 2003;31:1007-1014.
- Harigai R, Sakai S, Nobusue H, et al. Tranilast inhibits the expression of genes related to epithelial-mesenchymal transition and angiogenesis in neurofibromin-deficient cells. *Sci Rep*. 2018;8:6069.
- Kokuryo T, Yokoyama Y, Nagino M. Recent advances in cancer stem cell research for cholangiocarcinoma. *J Hepatobiliary Pancreat Sci*. 2012;19:606-613.
- Arima Y, Hayashi H, Sasaki M, et al. Induction of ZEB proteins by inactivation of RB protein is key determinant of mesenchymal phenotype of breast cancer. *J Biol Chem*. 2012;287:7896-7906.
- Manohar R, Komori J, Guzik L, et al. Identification and expansion of a unique stem cell population from adult mouse gallbladder. *Hepatology*. 2011;54:1830-1841.
- DiPaola F, Shivakumar P, Pfister J, Walters S, Sabla G, Bezerra JA. Identification of intramural epithelial networks linked to peribiliary glands that express progenitor cell markers and proliferate after injury in mice. *Hepatology*. 2013;58:1486-1496.
- Lanzoni G, Cardinale V, Carpino G. The hepatic, biliary, and pancreatic network of stem/progenitor cell niches in humans: A new reference frame for disease and regeneration. *Hepatology*. 2016;64:277-286.
- Fan B, Malato Y, Calvisi DF, et al. Cholangiocarcinomas can originate from hepatocytes in mice. *J Clin Invest*. 2012;122:2911-2915.
- Sekiya S, Suzuki A. Intrahepatic cholangiocarcinoma can arise from Notch-mediated conversion of hepatocytes. *J Clin Invest*. 2012;122:3914-3918.
- Guest RV, Boulter L, Kendall TJ, et al. Cell lineage tracing reveals a biliary origin of intrahepatic cholangiocarcinoma. *Can Res*. 2014;74:1005-1010.

39. Shiao MS, Chiablaem K, Charoensawan V, Ngamphaiboon N, Jinawath N. Emergence of intrahepatic cholangiocarcinoma: how high-throughput technologies expedite the solutions for a rare cancer type. *Front Genet.* 2018;9:309.
40. Otsuki Y, Saya H, Arima Y. Prospects for new lung cancer treatments that target EMT signaling. *Dev Dyn.* 2018;247:462-472.
41. Gonzalez DM, Medici D. Signaling mechanisms of the epithelial-mesenchymal transition. *Sci Sign.* 2014;7:re8.
42. Vaquero J, Guedj N, Claperon A, Nguyen Ho-Bouidoires TH, Paradis V, Fouassier L. Epithelial-mesenchymal transition in cholangiocarcinoma: From clinical evidence to regulatory networks. *J Hepatol.* 2017;66:424-441.
43. Nitta T, Mitsuhashi T, Hatanaka Y, et al. Prognostic significance of epithelial-mesenchymal transition-related markers in extrahepatic cholangiocarcinoma: comprehensive immunohistochemical study using a tissue microarray. *Br J Cancer.* 2014;111:1363-1372.
44. Sharma SV, Haber DA, Settleman J. Cell line-based platforms to evaluate the therapeutic efficacy of candidate anticancer agents. *Nat Rev Cancer.* 2010;10:241-253.
45. Shamir ER, Ewald AJ. Three-dimensional organotypic culture: experimental models of mammalian biology and disease. *Nat Rev Mol Cell Biol.* 2014;15:647-664.
46. Broutier L, Mastrogianni G, Verstegen MM, et al. Human primary liver cancer-derived organoid cultures for disease modeling and drug screening. *Nat Med.* 2017;23:1424-1435.
47. Saito Y, Nakaoka T, Muramatsu T, et al. Induction of differentiation of intrahepatic cholangiocarcinoma cells to functional hepatocytes using an organoid culture system. *Sci Rep.* 2018;8:2821.
48. van de Wetering M, Francies HE, Francis JM, et al. Prospective derivation of a living organoid biobank of colorectal cancer patients. *Cell.* 2015;161:933-945.
49. Nanki K, Toshimitsu K, Takano A, et al. Divergent routes toward Wnt and R-spondin niche independency during human gastric carcinogenesis. *Cell.* 2018;174(4):856-869.e17.
50. Seino T, Kawasaki S, Shimokawa M, et al. Human pancreatic tumor organoids reveal loss of stem cell niche factor dependence during disease progression. *Cell Stem Cell.* 2018;22(3):454-467.e6.
51. Fujii M, Shimokawa M, Date S, et al. A colorectal tumor organoid library demonstrates progressive loss of niche factor requirements during tumorigenesis. *Cell Stem Cell.* 2016;18:827-838.
52. Kerr EM, Gaude E, Turrell FK, Frezza C, Martins CP. Mutant Kras copy number defines metabolic reprogramming and therapeutic susceptibilities. *Nature.* 2016;531:110-113.
53. Merrick BA, Phadke DP, Bostrom MA, et al. Arsenite malignantly transforms human prostate epithelial cells in vitro by gene amplification of mutated KRAS. *PLoS One.* 2019;14:e0215504.
54. Hoadley KA, Yau C, Hinoue T, et al. Cell-of-origin patterns dominate the molecular classification of 10,000 tumors from 33 types of cancer. *Cell.* 2018;173:291-304.e6.
55. Huang WC, Tsai CC, Chan CC. Mutation analysis and copy number changes of KRAS and BRAF genes in Taiwanese cases of biliary tract cholangiocarcinoma. *J Formos Med Assoc.* 2017;116:464-468.

SUPPORTING INFORMATION

Additional supporting information may be found online in the Supporting Information section.

How to cite this article: Kasuga A, Semba T, Sato R, et al. Oncogenic KRAS-expressing organoids with biliary epithelial stem cell properties give rise to biliary tract cancer in mice. *Cancer Sci.* 2021;112:1822-1838. <https://doi.org/10.1111/cas.14703>